

Toward the Nanoscopic “Electronic Nose”: Hydrogen vs Carbon Monoxide Discrimination with an Array of Individual Metal Oxide Nano- and Mesowire Sensors

Victor V. Sysoev,[†] Bradly K. Button,[‡] Kelly Wepsiec,[‡] Serghei Dmitriev,[‡] and Andrei Kolmakov^{*,‡}

Department of Physics, Saratov State Technical University, Saratov 410054, Russia, and Physics Department, Southern Illinois University, Carbondale, Illinois 62901-4401

Received January 25, 2006; Revised Manuscript Received June 9, 2006

ABSTRACT

The array of chemiresistors made of individual pristine SnO₂, surface doped (Ni)-SnO₂ nanowires, and TiO₂ and In₂O₃ mesoscopic whiskers was fabricated on a Si/SiO₂ wafer. Their conductance was measured under pulses of H₂ and CO reducing gases in oxygen as background gas. The nanostructures were shown to be n-type semiconductors possessing high sensitivity to the target gases. Following the “electronic nose” concept, correlation analysis of response of three-chemiresistor array is shown to be sufficient to discriminate between H₂ and CO signals.

For the past few years a great variety of metal oxide quasi-one-dimensional (1D) nanostructures have been synthesized (see recent reviews^{1,2} and references therein), and a number of groups have been testing these nanostructures’ gas-sensitive properties against the range of reducing and oxidizing gases.^{3–11} As in traditional semiconductors the chemisorbed gas species induce near the surface space charge region (SCR) which becomes depleted (enriched) with electrons or holes in comparison with bulk equilibrium. Due to enhanced surface-to-bulk ratio and because the characteristic diameters of these nanostructures are comparable to the width of SCR, quasi-1D metal oxides demonstrate an excellent sensing performance¹² which is comparable or even better compared to the best thin film counterparts. Single-crystal quasi-1D nanostructures are particularly good prospects for chemical sensing applications where the large-scale integration, reproducibility, and aging performance are important since their dimensions and high sensitivity are complemented with robust and well-defined morphology, surface faceting, and stoichiometry. However, these nanosensors inherited the insufficient selectivity of macroscopic oxide sensors, a challenge which still remains unresolved.¹³ A variety of methods were developed in macroscopic oxide

sensors to improve their selectivity, including, for example, particular bulk (or surface) doping, operating temperature cycling or lateral thermal gradients, the application of gas specific prefilters, etc.

Alternatively, the principally different approach is to read out a signal from the array of individual sensors with overlapping but different (i.e., orthogonal) gas sensitivity. Instead of identifying the specific target gas with an individual sensor, the response of an entire array carries the “fingerprints” or “image” of the gas mixture and is potentially more redundant and fault tolerant. The response of such a sensing net toward complex gas mixtures and odors relies on well-developed pattern recognition techniques.^{14–16} The devices based on these sensing arrays are frequently referred to as “electronic noses” because they mimic the principle of the mammalian olfactory system (see refs 14–16 and references therein).

The present Letter is a comparative study of gas-sensing properties of individual SnO₂, In₂O₃, and TiO₂ nano- and mesowires placed on the same chip and wired as an array of chemiresistors. We report the data on gas sensing toward oxygen (as a model oxidizing agent) and its mixture with two model reducing gases (hydrogen and carbon monoxide) and demonstrate the feasibility of this nanostructure array as a promising path toward the development of a robust “nanoelectronic nose” device.

* Corresponding author. E-mail: akolmakov@physics.siu.edu.

[†] Saratov State Technical University.

[‡] Southern Illinois University.

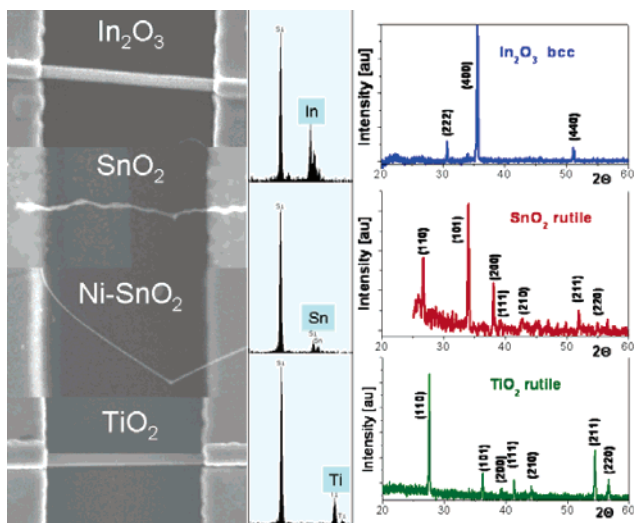


Figure 1. (left panel) SEM micrograph of metal oxide nano- and mesowires taken from three corresponding areas of the sample: top and bottom, In_2O_3 and TiO_2 mesoscopic rods, respectively, in the middle, $-\text{SnO}_2$ segmented nanostructure and Ni surface doped SnO_2 nanowire (see also the comment in ref 32). Compositional (middle panel) and structural (right panel) analysis of the nanostructures performed using EDX and XRD techniques. The interelectrode distance is $12 \mu\text{m}$.

Single-crystal nano- and mesowires of SnO_2 , TiO_2 , and In_2O_3 were synthesized via a vapor–solid method (VS) using only slight deviations from previously reported protocols.^{17,18} To achieve diversity in the gas response, the surface of one of two SnO_2 nanostructures employed in the study was functionalized in situ with Ni catalyst nanoparticles using the method described earlier.¹⁹

The morphology, composition, stoichiometry, and structure of the synthesized oxide nanowires and whiskers were examined using a scanning electron microscope (SEM) (Hitachi S2460N) equipped with an energy dispersive X-ray (EDX) detector (NORAN Voyager III) and also using X-ray diffraction (XRD) analysis on nanowire mats.

Figure 1 depicts SEM images, EDX and XRD data of mesoscopic whiskers, and nanowires used in this study. The different morphology of these structures is a positive factor which, along with the compositional divergence, contributes to a specificity of the response to the particular gas. The effective diameters (see comment in ref 32) of the nanostructures, D , were in the order of 100 nm for tin oxide nanowires, and ca. 1000 nm for the titanium and indium oxide whiskers. XRD reflexes from the titanium oxide nanostructures are in agreement with diffraction data²⁰ which correspond to the tetragonal rutile structure. The spectrum of tin oxide contains major reflexes from (110), (101), (200) lattice planes, which identifies the nanostructure as SnO_2 rutile crystals.²⁰ The indium oxide spectrum has peaks indexed as (222), (400), (440), (622) lattice planes which, in turn, identify the whiskers to be In_2O_3 body-centered cubic (bcc) crystal.²⁰ It is worth noting that relative intensities of peaks in XRD spectra of the nanostructures deviate from the standard powder ones. The latter is due to a preferential growth of the nanowires in a certain direction.

Three separate areas with low densities of SnO_2 , TiO_2 , In_2O_3 nanowires were created on a commercial $5 \times 5 \text{ mm}^2$ Si:SiO₂ wafer. The array of Ti/Au, 40/300 nm thick, contact pads was deposited over these three areas using a resist free shadow mask evaporation method. The individual SnO_2 , TiO_2 , In_2O_3 nanowire chemiresistors with well-defined contacts were determined using SEM or a high-resolution optical microscope. The space between the contact pads, shown in Figure 1, is $12 \mu\text{m}$. The sample was mounted in the holder inside the custom-made variable pressure and temperature probe station for conductometric measurements. The details of the station can be found in ref 33. Briefly, the probe station with basic pressure up to 10^{-7} Pa is equipped with micromanipulators and computer-controlled pulsed valves. By regulation of the pulse structure and needle valves, the total pressure and mixture composition of the target and background gases can be tuned. The substrate holder is equipped with a resistive heater capable of operating up to 1200 K. In this particular set of measurements the array of nanostructures was kept at 623 K to speed up adsorption/desorption kinetics. Ni source was used to functionalize in situ the surface of one of the SnO_2 nanowire chemiresistors with the catalyst.¹⁹ The conductance measurements during the metal deposition were used to ensure an absence of the percolation between Ni nanoparticles on the surface of SnO_2 . In a separate test it was observed that the deposited nanoparticles were covered with a thin layer of NiO which is manifested in p-type conductance when thin film is formed (see ref 33).

The measurements of the nanostructures' conductance were performed: (i) under high vacuum conditions, (ii) while admitting pure oxygen as oxidizing background gas up to a pressure of 1.3×10^{-2} Pa, and (iii) during pulses of H_2 and CO having oxygen as a background gas. All the pressure readings were corrected to the gauge sensitivity factor of the particular gas. The percentage of reducing gas (H_2 and CO) in the mixture was driven by adjusting the ON/OFF pulse structure of the corresponding valves. To check the linearity of the response, two different concentrations of reducing gases were chosen which, along with 1.3×10^{-2} partial pressure of oxidizing background, made the total pressure in the vacuum chamber during these measurements 2.6×10^{-2} and 4×10^{-2} Pa.

After the array was heated to the operating temperature in a vacuum but prior to starting the measurements, the I – V curves were measured for each nanostructure to ensure the Ohmic character of the contacts (Figure 2). As one can see from Figure 2, the thicker structures have higher absolute values of the conductance roughly obeying a $I \sim D^2$ trend.

The oxygen admission led to a decrease of conductance of all the nanowires indicating their n-type behavior. The largest change in conductance, about an order of magnitude, upon 1.3×10^{-2} Pa oxygen exposure was observed in the case of a SnO_2 nanowire functionalized with Ni(NiO) nanoparticles. The sequential exposure of the nanostructures to hydrogen pulses showed a reproducible and pronounced increase of the conductance for all the structures (Figure 3). Similar responses were observed in the case of carbon

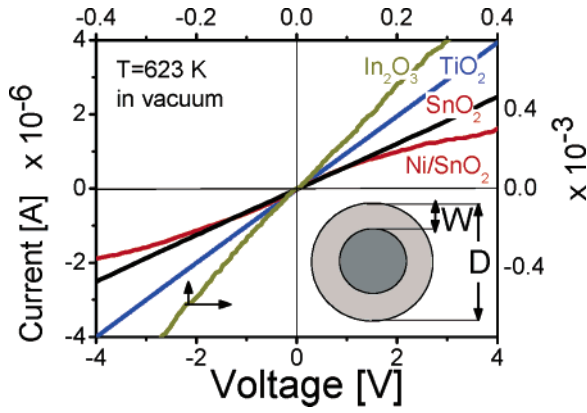


Figure 2. Current–voltage characteristics taken on individual metal oxide nanostructures in a vacuum at 623 K. Right-top scales correspond to highly conductive In_2O_3 nanowhisker. The insert diagram represents the effective cross section of the nanostructure where W is the width of the depletion zone.

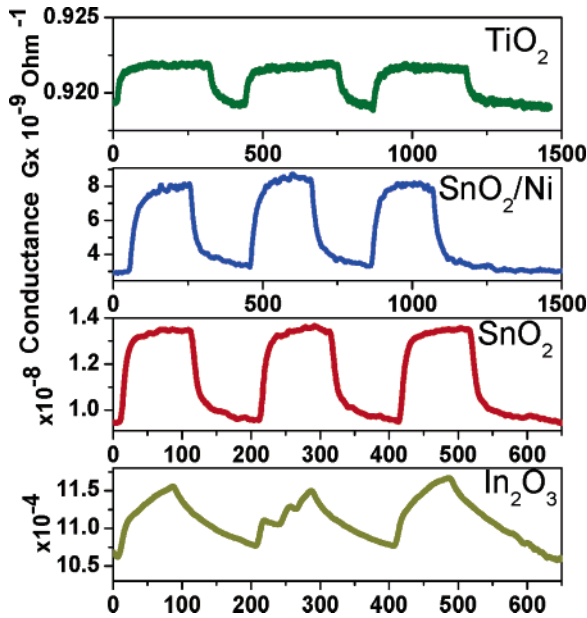


Figure 3. The response of the array of the chemiresistors to three consecutive hydrogen pulses with partial pressure of 6.4×10^{-2} Pa. The background conductance is measured under the constant oxygen pressure of 1.3×10^{-2} Pa

monoxide pulses with an exception of the indium oxide whisker. At the chosen range of concentrations, CO did not cause a measurable change in conductance in this mesowire. In addition, the In_2O_3 whisker response to hydrogen was slower than that for any of the other structures. These particular observations presumably result from the large diameter of this whisker’s conducting channel which apparently cannot be effectively modulated by the surface processes such as oxygen chemisorption and CO oxidation reaction. On the other hand, dissociation and facile diffusion of hydrogen can change the doping level through the entire bulk of this mesowire and therefore account for the observed conductance changes.

Due to the In_2O_3 structure’s minute sensitivity toward CO and slow response to hydrogen, further measurements on the chemiresistor array were limited by three nanostructures of

Table 1. The Measured Responses of the Nanowires to Reducing Gases, %

gas	partial pressure ^a $\times 10^{-2}$ Pa	nanostructure		
		SnO_2	$\text{SnO}_2:\text{Ni}$	TiO_2
H_2	3.2	24.1	131.7	0.41
	6.4	39.5	253.2	0.59
CO	1.2	12.2	25	0.16
	2.5	16.1	46.8	0.32

^a The values are corrected accounting for a calibration factor of penning ionization gauge.

SnO_2 , SnO_2/Ni , and TiO_2 . The response of the chemiresistors was defined as

$$S = \frac{G_g - G_O}{G_O} \quad (1)$$

where G_g and G_O are the nanostructure conductance under the reducing gas mixed with oxygen and under pure oxygen background, respectively. The results of measurements at 623 K are summarized in Table 1.

The basic principle of responsiveness of the conductance in these quasi-1D structures toward chemisorbed species relies on the fact that the gas species chemisorbed on the oxide surface change the number of free carriers within SCR while the rest of the oxide bulk remains unaffected. The differences in the observed gas responses therefore would obey roughly the degree of adsorbate induced depletion/accumulation in the nanostructure’s SCR with respect to its diameter.

By acceptance of the coaxial geometry as a first approximation of the conducting channel (see insert in the Figure 2), the conductance through the nanostructure in an oxidizing environment is

$$G_O = n_0 e \mu \frac{\pi(D - 2W)^2}{4d} \quad (2)$$

where n_0 is the carrier’s concentration in the conducting channel, e the elementary charge, μ the carrier mobility, d the length of the chemiresistor, and W the width of SCR which is depleted with electrons. Assuming W to be still significantly smaller than D for our structures, one can show that response

$$S \approx \frac{4W}{D} \quad (3)$$

i.e., is proportional to the ratio of SCR width to the diameter of the structure. To estimate SCR width

$$W = L_D \left(\frac{eV_S}{kT} \right)^{1/2} \quad (4)$$

one has to evaluate the adsorbate-induced band bending V_S and the Debye length L_D . The latter one: $L_D = (\epsilon \epsilon_0 kT / e^2 n_0)^{1/2}$

Table 2. The Calculated Concentration of Free Carriers and Effective Debye Length in Oxide Nanostructures

	SnO ₂	SnO ₂ :Ni	TiO ₂
n_0, cm^{-3}	$\sim 5 \times 10^{17}$	$\sim 1 \times 10^{16}$	$\sim 2 \times 10^{18}$
L_D, nm	~ 10	~ 70	~ 10

(here ϵ_0 the absolute dielectric constant, ϵ the relative dielectric permittivity of the structure, k the Boltzmann's constant, T the working temperature in K) in fact is determined by concentration of oxygen vacancies which are dominant point defects in SnO₂ and TiO₂.²¹ The vacancies induce shallow donor states in the oxides gap rather close to the conduction band edge²² which might be considered to be fully ionized²³ under operating temperatures about 623 K. The concentration of free carriers can be determined from $I(V)$ measurements of the conductance at high vacuum conditions using formula (2) under conditions $W = 0$. Adopting the mobility data known for bulk oxide single crystals^{24–28} as μ_n to be equal to 80 and 1 cm²/(V s), and ϵ to be equal to 15 and 70, respectively, for SnO₂ and TiO₂ crystals, one can get results for n_0 and L_D (see Table 2).

Assuming V_s is typically in the order of 0.1 eV under such exposure levels and keeping in mind that kT is ca. 0.052 eV at the operation temperature, one can consider $W \sim L_D$ as a feasible approximation. Under these simplistic assumptions and using calculated L_D from Table 2, the estimated values for S for SnO₂, SnO₂:Ni, and TiO₂ would be ca. 40, 260, and 4%. Despite the above rough assumptions, these data not only nicely match the relative ratio between measured responses S but also reasonably well predict their absolute values at higher surface coverages by gas adspecies (as is the case of hydrogen input at a pressure of 6.4×10^{-2} Pa). This argues in favor of a simple coaxial depletion picture summarized by formula (3) and all related assumptions.

From transport and sensing measurements one can notice significantly elevated gas responses and L_D values obtained for SnO₂:Ni in comparison with other chemiresistors. Provided that these functionalized and pristine SnO₂ nanostructures have comparable dimensions, the large differences in L_D and sensitivity properties between these two structures apparently come from the Ni (or NiO) doping effect. In conjunction with Ni doping results obtained for thin film sensors²⁹ and our own TEM studies of Ni deposits on SnO₂ nanowires, surface Ni atoms being accommodated at the tin oxide surface form small Ni clusters which become (at least at the surface) oxidized to possess p-type NiO properties (see ref 33). This p-type semiconductor dopes n-SnO₂ with holes that leads to an additional near surface compensation of a number of available donors. The reduced number of available carriers in the SnO₂:Ni nanowire allows the chemisorption of gas to affect the entire nanowire volume leading to higher gas sensitivity. Conversely, the ratio between L_D and D is smaller in the pristine SnO₂ nanowire and results in only partial depletion. A similar situation occurs in the TiO₂ whisker; thus the gas adsorption on SnO₂ and TiO₂ nano-(meso)structures affects mainly the space charge region of about L_D deep leaving the free carrier concentration in the conducting channel unchanged.³⁰ The detailed comparative

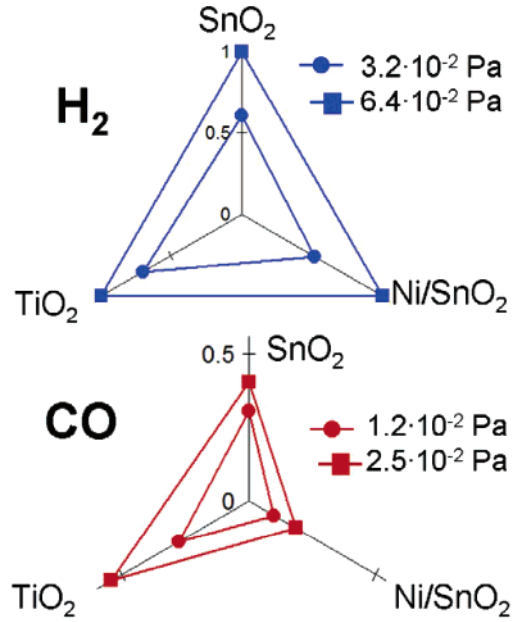


Figure 4. The response of a three-chemiresistor array to H₂ (top) and CO (bottom) inputs, normalized by maximum value.

analysis of the sensing performance of pristine and doped oxide nanowires is a subject of ongoing studies.

Both hydrogen and carbon monoxide increase the conductance of the chemiresistors, and the magnitude of this change is controlled by the surface reactivity to the specific gas and also by gas concentration.³⁴ Thus, as in the case of thin film sensors, the selectivity of the individual nanostructure is not sufficient to discriminate between them. However the gas recognition can be achieved using well-established methods realized for “electronic noses”.^{14–16} Namely, signal patterns can be depicted for these three sensing elements as radial plots: each radial beam shows the signal of one single sensing element normalized to its maximum value. As can be seen from Figure 4, the radial plots of H₂ and CO gas responses over the chemiresistor array are prominently different for two gases. This visual difference is supported by results achieved by processing the data with simple correlation analysis performed in accordance with a simple algorithm (see ref 31 as an example). This analysis indicates that the nanostructure array responses to hydrogen and carbon monoxide have only a slight correlation (the correlation coefficient is ca. 0.25). Therefore, while the single structures have no specific sensitive properties to these two test reducing gases, the array's response is rather selective. Apparently, increasing the number of nanostructures assembled as an array should lead to higher degree of gas discrimination.

In conclusion, we have synthesized individual SnO₂, SnO₂:Ni nanowires, and TiO₂ and In₂O₃ mesoscopic whiskers and assembled them as an array of chemiresistors on the single chip. The response of the active elements toward the minute concentrations of hydrogen and carbon monoxide mixed with oxygen was compared at 623 K. We have established that at tested size scale the differences of gas response of the nanowires in the first approximation are governed by a ratio

between the diameter of the nanostructure and its Debye length. It is demonstrated that a discrimination between H₂ and CO can be achieved using the electronic nose approach through an analysis of the responses from the three nanowire array. The obtained results can be used for further development of a real world “nanoscopic E-nose” based on the array of individual metal oxide quasi-1D nanostructures. The methodology used in this study can be easily transferred to already reported “real world” sensor prototypes which are based on quasi-1D metal oxide nanostructures.^{35,36}

Acknowledgment. Authors are thankful to Dr. Y. Lilach (PNNL), Mr. C. Watts for the help with experiment, and Professor S. Stadler, Mr. J. Mitchell, and Mr. S. Schmitt (IMAGE center) for their help with sample characterization. The research was supported by a SIUC Faculty Seed Grant and partially through the SIUC Materials Technology Center. V.S. thanks the Russian Agency for Science & Innovations for a travel grant, Contract No. 02.444.11.7022. Some valuable equipment used in this study was generously donated to A.K. by Professor M. Moskovits (UCSB).

Supporting Information Available: Description of resist free fabrication of the array of nanowire chemiresistors on a single Si/SiO₂ chip, the multifunctional ultrahigh vacuum probe station, and in situ SnO₂ nanowire surface functionalization with NiO. This material is available free of charge via the Internet at <http://pubs.acs.org>.

References

- (1) Dai, Z. R.; Pan, Z. W.; Wang, Z. L. *Adv. Funct. Mater.* **2003**, *13*, 9–24.
- (2) Xia, Y. N.; Yang, P. D.; Sun, Y. G.; Wu, Y. Y.; Mayers, B.; Gates, B.; Yin, Y. D.; Kim, F.; Yan, Y. Q. *Adv. Mater.* **2003**, *15*, 353–389.
- (3) Cui, Y.; Wei, Q. Q.; Park, H. K.; Lieber, C. M. *Science* **2001**, *293*, 1289–1292.
- (4) Law, M.; Kind, H.; Messer, B.; Kim, F.; Yang, P. D. *Angew. Chem., Int. Ed.* **2002**, *41*, 2405–2408.
- (5) Comini, E.; Faglia, G.; Sberveglieri, G.; Pan, Z. W.; Wang, Z. L. *Appl. Phys. Lett.* **2002**, *81*, 1869–1871.
- (6) Arnold, M. S.; Avouris, P.; Pan, Z. W.; Wang, Z. L. *J. Phys. Chem. B* **2003**, *107*, 659–663.
- (7) Kolmakov, A.; Zhang, Y. X.; Cheng, G. S.; Moskovits, M. *Adv. Mater.* **2003**, *15*, 997–1000.
- (8) Li, C.; Zhang, D. H.; Liu, X. L.; Han, S.; Tang, T.; Han, J.; Zhou, C. W. *Appl. Phys. Lett.* **2003**, *82*, 1613–1615.
- (9) Wang, Y. L.; Jiang, X. C.; Xia, Y. N. *J. Am. Chem. Soc.* **2003**, *125*, 16176–16177.
- (10) Fan, Z. Y.; Lu, J. G. *Appl. Phys. Lett.* **2005**, *86*, 123510.
- (11) Murray, B. J.; Newberg, J. T.; Walter, E. C.; Li, Q.; Hemminger, J. C.; Penner, R. M. *Anal. Chem.* **2005**, *77*, 5205–5214.
- (12) Zhang, D. H.; Liu, Z. Q.; Li, C.; Tang, T.; Liu, X. L.; Han, S.; Lei, B.; Zhou, C. W. *Nano Lett.* **2004**, *4*, 1919–1924.

- (13) Kolmakov, A.; Moskovits, M. *Annu. Rev. Mater. Res.* **2004**, *34*, 151–180.
- (14) Persaud, K.; Dodd, G. *Nature* **1982**, *299*, 352–355.
- (15) Albert, K. J.; Lewis, N. S.; Schauer, C. L.; Sotzing, G. A.; Stitzel, S. E.; Vaid, T. P.; Walt, D. R. *Chem. Rev.* **2000**, *100*, 2595–2626.
- (16) *Handbook of Machine Olfaction*; Pearce, T. C., Nagle, H. T., Gardner J. W., Eds.; Wiley-VCH: Weinheim, 2003.
- (17) Lilach, Y.; Zhang, J. P.; Moskovits, M.; Kolmakov, A. *Nano Lett.* **2005**, *5*, 2019–2022.
- (18) Kalinin, S. V.; Shin, J.; Jesse, S.; Geohegan, D.; Baddorf, A. P.; Lilach, Y.; Moskovits, M.; Kolmakov, A. *J. Appl. Phys.* **2005**, *98*, 044503.
- (19) Kolmakov, A.; Klenov, D. O.; Lilach, Y.; Stemmer, S.; Moskovits, M. *Nano Lett.* **2005**, *5*, 667–673.
- (20) *Powder diffraction File. Data Cards. Inorganic Section*; JCPDS: Swarthmore, PA, 1987; 21-1276, 41-1445, 6-0416.
- (21) Kohl, D. *J. Phys. D: Appl. Phys.* **2001**, *34*, R125–R149.
- (22) Cox, D. F.; Fryberg, T. B.; Semancik, S. *Phys. Rev. B* **1988**, *38*, 2072–2083, and references therein.
- (23) *Semiconductor sensors in physical-chemical studies*; Kupriyanov, L. Yu., Ed.; Elsevier: Amsterdam, 1996; p 29.
- (24) Marley, J. A.; Dockerty, R. C. *Phys. Rev.* **1965**, *140A*, 304–310.
- (25) Breckenridge, R. G.; Hosler, W. R. *Phys. Rev.* **1953**, *91*, 793–802.
- (26) Grant, F. A. *Rev. Mod. Phys.* **1959**, *31*, 646–674.
- (27) Parker, R. A. *Phys. Rev.* **1961**, *124*, 1719–1722.
- (28) Jarzebski, Z. M.; Marton, J. P. *J. Electrochem. Soc.* **1976**, *123*, 299–310C.
- (29) Ma, Y. J.; Zhou, F.; Lu, L.; Zhang, Z. *Solid State Commun.* **2004**, *130*, 313–316.
- (30) Wolkenstein, T. *Electronic processes on semiconductor surfaces during chemisorption*; Consultants Bureau: New York, 1991.
- (31) Muller, R. Multisensor Signal Processing. In *Sensors: a comprehensive survey. Vol.1, Fundamentals and general aspects*; Goepel, W., Hesse, J., Zemel, J. N., Grandke, T., Ko, W. H., Eds.; VCH: Weinheim, 1989; pp 313–330.
- (32) To induce as much orthogonality in the gas response as possible, the usage of the morphological different nanostructures is a favorable factor. In the device in Figure 1 we have used segmented SnO₂ nanowires which have sequential thin (ca. 70 nm) and thick (ca. 400 nm) segments (ref 17). The electron transport and therefore sensing performance is controlled by thinner segments. On the basis of the SEM images, we approximate an effective diameter of the conducting channel in a vacuum for this nanostructure to be ca. 100 nm. The second straight Ni–SnO₂ nanostructure has a kink since the nanowire changed growth direction during fabrication, which in principle is able to dominate the performance of the chemiresistor. It turns out that the kink appears not to be an electroactive defect and did not disturb neither Ohmic behavior nor expected value of the conductance. The plausible explanation is that the nanostructure’s diameter is ca. 100 nm and therefore the scattering effects due to surface and/or morphology inhomogeneities have a minor effect.
- (33) See Supporting Information.
- (34) *Techniques and Mechanisms in Gas Sensing*; Moseley, P. T., Norris, J., Williams, D., Eds.; The Adam Hilger Series on Sensors; Adam Hilger: Bristol, 1991.
- (35) Paulose, M.; Varghese, O. K.; Mor, G. K.; Grimes, C. A.; Ong, K. G.; *Nanotechnology* **2006**, *17* (2), 398–402.
- (36) Wang, H. T.; Kang, B. S.; Ren, F.; Tien, L. C.; Sadik, P. W.; Norton, D. P.; Pearton, S. J.; Lin, J. *Appl. Phys. Lett.* **2005**, *86* (24), No. 243503.

NL060185T